Journal of Marine Science and Technology

Volume 24 | Issue 4 Article 15

DYNAMIC SIMULATION OF SUBSEA EQUIPMENT INSTALLATION USING AN OFFSHORE SUPPORT VESSEL BASED ON FLEXIBLE MULTIBODY SYSTEM DYNAMICS

Jeong-Woo Hong
Researcher, Offshore Engineering Research Department, Hyundai Heavy Industries, 1000, Bangeojinsunhwan-doro, Dong-gu, Ulsan, Republic of Korea

Myung-Il Roh
Associate Professor, Department of Naval Architecture and Ocean Engineering, and Research Institute of Marine Systems Engineering, Seoul National University, 1 Gwanak-ro, Gwanak-gu, Seoul, Republic of Korea., miroh@snu.ac.kr

Seung-Ho Ham
Researcher, Offshore Engineering Research Department, Hyundai Heavy Industries, 1000, Bangeojinsunhwan-doro, Dong-gu, Ulsan, Republic of Korea

Sol Ha
Assistant Professor, Department of Ocean Engineering, Mokpo National University, Muan-gun, Republic of Korea.

DYNAMIC SIMULATION OF SUBSEA EQUIPMENT INSTALLATION USING AN OFFSHORE SUPPORT VESSEL BASED ON FLEXIBLE MULTIBODY SYSTEM DYNAMICS

Acknowledgements

This study was partially supported by (a) BK21 Plus Program (Education and Research Center for Creative Offshore Plant Engineers) funded by the Ministry of Education of the Republic of Korea; and (b) Research Institute for Marine Systems Engineering of Seoul National University, Republic of Korea.

Journal of Marine Science and Technology, Vol. 24, No. 4, pp. 807-821 (2016)
DOI: 10.6119/JMST-016-0323-1

DYNAMIC SIMULATION OF SUBSEA EQUIPMENT INSTALLATION USING AN OFFSHORE SUPPORT VESSEL BASED ON FLEXIBLE MULTIBODY SYSTEM DYNAMICS

Jeong-Woo Hong[1], Myung-Il Roh[2], Seung-Ho Ham[1], and Sol Ha[3]

Key words: offshore supply vessel, dynamic simulation, flexible multibody system dynamics, crane lifting, subsea equipment installation.

ABSTRACT

An offshore support vessel (OSV) is a ship that supports exploration, development, and production activities in the offshore industry. Recently, industrial demand for OSVs has increased due to a large number of offshore field development projects worldwide. One of the main functions of an OSV is heavy lifting such as subsea equipment installations in offshore oil or gas fields using crane. Therefore, predicting dynamic loads in various operation conditions is one of the crucial points in the lifting operation of an OSV. To do this, crane-lifting simulation needs to precede real operation to verify the safety of the lifting operation. Most simulation tools use a rigid body model for crane-lifting simulation. However, in real cases, some heavy loaded components such as crane boom might be deformed due to their own weight and the weight of the lifted object. The deformation can change during the lifting operation because ship motion induced by ocean waves and winds can affect the overall behavior of the OSV. This study derives equations for the motion of a multibody system using a flexible body model for the crane boom based on finite element formulation to analyze the behavior of the system, dynamic loads, and the deformation of the crane boom under various ocean conditions. Motion equations were solved with fourth-order Runge-Kutta method. Our results showed that flexible body models had bigger dynamic amplification factors than rigid body models in all cases, indicating that the flexibility of the crane boom should be considered for accurate estimation of the dynamic effect on OSV lifting simulation. Finally, we can find operability of the lifting operation at given ocean conditions.

I. INTRODUCTION

1. Background

An offshore support vessel (OSV) is a vessel that provides support for exploration, development, and production activities in the offshore industry. Recently, industrial demand for OSVs has increased due to a large number of offshore field development projects worldwide. An OSV has five main roles: supporting platforms, subsea operation and construction, heavy lifting, provision of crew residence, and exploration (Park et al., 2012). To perform these roles, most OSVs have a heavy-lifting crane on their deck. The heavy-lifting crane can load and unload supplies to support the installation of offshore platforms and subsea equipment such as manifolds (Woo, 2014). For crane operation in an ocean environment, dynamic analysis and lifting simulation are required to predict dynamic loadings on the equipment and accurate lowering position for safety purposes (Cha et al., 2010a).

OSV during its lifting operation can be modeled with a multibody system consisting of a number of bodies and joints with constraints. Fig. 1 shows the configuration of an OSV multibody model. The bodies for crane-lifting simulation can be modeled with four components: an OSV hull with hydrodynamic and static forces, a crane tower connected to the hull by a rigid fixed joint, a crane boom connected to the crane tower by a fixed or hinge joint, and the lifted object connected to the crane boom by a wire rope.

In most past lifting simulations, each component was regarded as a rigid body. However, in real cases, some heavy loaded components such as crane boom are deformed due to their own weight and the weight of the lifted object. The

Paper submitted 03/06/15; revised 11/26/15; accepted 03/23/15. Author for correspondence: Myung-Il Roh (e-mail: miroh@snu.ac.kr).
[1] *Researcher, Offshore Engineering Research Department, Hyundai Heavy Industries, 1000, Bangeojinsunhwan-doro, Dong-gu, Ulsan, Republic of Korea.*
[2] *Associate Professor, Department of Naval Architecture and Ocean Engineering, and Research Institute of Marine Systems Engineering, Seoul National University, 1 Gwanak-ro, Gwanak-gu, Seoul, Republic of Korea.*
[3] *Assistant Professor, Department of Ocean Engineering, Mokpo National University, Muan-gun, Republic of Korea.*

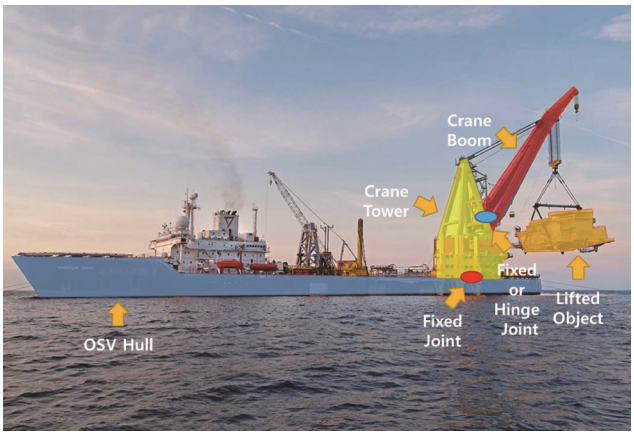

Fig. 1. Configuration of the multibody model of an offshore support vessel (OSV).

deformation can change during the lifting operation because ship motion induced by ocean waves and wind can affect the overall behavior of the multibody system. In this study, equations of motion of the multibody system are derived using a flexible body model for the crane boom based on the finite element formulation to analyze the behavior of the system (Shabana, 2005), its dynamic loads, and the deformation of the crane boom under various ocean conditions. Equations of motion are solved using the fourth-order Runge-Kutta method. Finally, all results are compared to those obtained from a rigid body model to validate the flexible model in dynamic simulation of an OSV.

2. Related Studies

Al-Sweiti and Soffker (2007) used an elastic model for a crane boom divided into five finite elements. Pointed mass model was used for the load. The hull structure had a one-degree-of-freedom body with only a rolling motion. The equations of motion were derived from Newton's motion equation. Ren et al. (2008) considered three degrees-of-freedom motions of a ship: its heave, surge, and pitch motions. The elasticity of the crane boom was considered as an additional displacement of the crane tip. The hydrostatic forces, mooring forces, water resistance due to the viscosity, and excitation force due to the ocean waves were considered as external forces. Park et al. (2010) used flexible multibody dynamics to derive equations of motion of a floating crane barge. The crane boom was modeled with an arbitrary number of three-dimensional (3D) finite elements. Halse et al. (2014) simulated crane lifting of an OSV coupled with analysis of hydrodynamic forces. They used a rigid body model and one degree-of-freedom of the ship motion. A brief summary and comparison of related studies are summarized in Table 1.

In this study, as in Park et al. (2010), the equations of motion of the OSV were derived based on flexible multibody dynamics. The crane boom was modeled with an arbitrary number of 3D finite elements. The remainder of this paper is structured as follows. Section 2 describes the derivation of

Table 1. Summary and comparison of related studies.

		Halse et al. (2014)	Park et al. (2010)	Ren et al. (2008)	Al-Sweiti and Soffker (2007)
Mathematical modeling		Rigid multibody dynamics coupled with hydrodynamics	Flexible multibody dynamics	Lagrange's equation	Newton's equation
Boom	No. of elements	-	N	-	5
	Elastic coordinates	-	Nodal	-	Nodal
DOF of the floating crane		1	6	3	1
DOF of the cargo		1	6	1	1
Lifted object		Rigid body	Rigid body	Point mass	Point mass
Automatic formulation		-	O	X	X
Simulation target		Crane on the OSV	Offshore crane on the crane barge	Offshore crane on the crane barge	Offshore crane on the crane barge

equations of motion of a flexible multibody system with finite element formulation. In Section 3, a comparative study of flexible multibody dynamics for a 2D cantilever beam is performed. Section 4 shows the results of the dynamic simulation of the lifting operation of an OSV based on flexible multibody dynamics. The last section summarizes the results of this study and briefly discusses the next study.

II. DERIVATION OF THE EQUATIONS OF MOTION OF THE FLEXIBLE MULTIBODY SYSTEM WITH FINITE ELEMENT FORMULATION

1. Kinematic Description of a Deformable Body

Shabana (2005) suggested the equations of motion of the flexible multibody system with finite element formulation. Finite element formulation uses four coordinates systems to describe arbitrary points on a deformable body in the global coordinate system. Fig. 2 shows the four coordinates systems used for the formulation. The superscript i refers to the body number in the multibody system. The superscript j refers to the element number in the finite element discretization of the deformable body i. Subscript i refers to the intermediate element coordinate system. A global coordinate system is fixed in time. It forms a single standard for the entire assembly of bodies. Thus, it expresses the connectivity of all bodies through the system. A body coordinate system forms a single standard for the entire assembly of elements in the body i thus expressing the connectivity of all elements in the body. An intermediate element coordinate system is a system whose origin is rigidly attached to the origin of the body coordinate

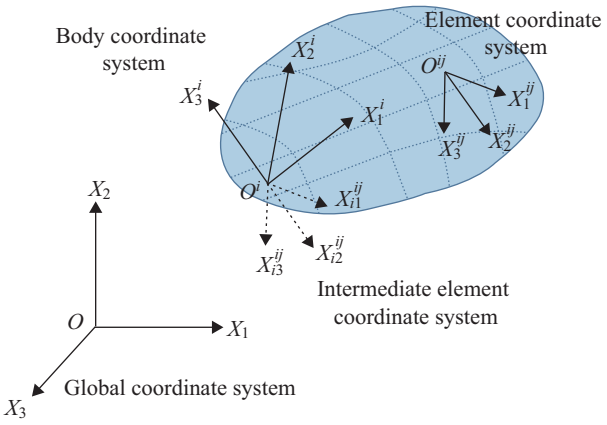

Fig. 2. Finite element coordinate systems.

Fig. 3. 3D nodal coordinates of a beam element.

system. it does not follow deformation of the element. The intermediate element coordinate system is initially oriented to be parallel to the element coordinate system. An element coordinate system is rigidly attached to each element *j* on the deformable body *i*. This coordinate system translates and rotates with the element. An arbitrary displacement vector with respect to the element coordinate system is shown as follows:

$$\mathbf{w}^{ij} = \mathbf{S}^{ij}\mathbf{e}^{ij}, \tag{1}$$

wherein $\mathbf{S}^{ij}$ is the element shape matrix and $\mathbf{e}^{ij}$ is the nodal coordinate of the element with respect to the element coordinate system. An explicit expression for shape matrix is defined in Appendix A1. The 3D nodal coordinates of a beam element are defined as follows. (Fig. 3).

However, an intermediate element coordinates system with a fixed orientation with respect to body coordinate parallel to the axis of the element coordinates system was introduced to transform the body coordinates system. Thus, the displacement vector with respect to the intermediate coordinates can be defined as follows:

$$\mathbf{w}_i^{ij} = \mathbf{S}^{ij}\mathbf{e}_i^{ij}, \tag{2}$$

wherein $\mathbf{w}_i^{ij}$ is the displacement vector and $\mathbf{e}_i^{ij}$ is the nodal coordinate of the element *ij* with respect to the intermediate element coordinates system. In addition, $\mathbf{e}_i^{ij}$ can be obtained from the vector of the nodal coordinates of element *ij* with respect to the body coordinates system $\mathbf{q}_n^{ij}$ using rotation transformation matrix $\bar{\mathbf{C}}^{ij}$ as follows.

$$\mathbf{e}_i^{ij} = \bar{\mathbf{C}}^{ij}\mathbf{q}_n^{ij} \tag{3}$$

The displacement vector $\bar{\mathbf{u}}^{ij}$ can be defined in the *i*-th body coordinates system as follows.

$$\bar{\mathbf{u}}^{ij} = \mathbf{C}^{ij}\mathbf{w}_i^{ij} = \mathbf{C}^{ij}\mathbf{S}^{ij}\mathbf{e}_i^{ij} = \mathbf{C}^{ij}\mathbf{S}^{ij}\bar{\mathbf{C}}^{ij}\mathbf{q}_n^{ij} \tag{4}$$

Eq. (4) defines the position coordinates of an arbitrary point on the finite element with respect to the origin of the body coordinates system. These position coordinates are expressed in terms of nodal coordinate sets defined in the body coordinates system.

If $\mathbf{q}_n^i$ is the total vector of the nodal coordinates of body *i* resulting from the finite element discretization, the vector of the element nodal coordinate can be written in terms of nodal coordinates of the body as follows:

$$\mathbf{q}_n^{ij} = \mathbf{B}_1^{ij}\mathbf{q}_n^i, \tag{5}$$

wherein $\mathbf{B}_1^{ij}$ is the element selection matrix whose elements are either zeros or one. An example is shown in Fig. 4, where body 1 is divided into two beam elements.

In the example in Fig. 4, total vector of the nodal coordinate $\mathbf{q}_n^1$ is defined as follows:

$$\begin{aligned}\mathbf{q}_n^1 = [&e_1^1 \quad e_2^1 \quad e_3^1 \quad e_4^1 \quad e_5^1 \quad e_6^1 \quad e_7^1 \quad e_8^1 \quad e_9^1 \\ &e_{10}^1 \quad e_{11}^1 \quad e_{12}^1 \quad e_{13}^1 \quad e_{14}^1 \quad e_{15}^1 \quad e_{16}^1 \quad e_{17}^1 \quad e_{18}^1]^{\mathrm{T}},\end{aligned} \tag{6}$$

and $\mathbf{q}_n^{11}$ and $\mathbf{q}_n^{12}$ are defined as follows:

$$\begin{aligned}\mathbf{q}_n^{11} = [&e_1^{11} \quad e_2^{11} \quad e_3^{11} \quad e_4^{11} \quad e_5^{11} \quad e_6^{11} \\ &e_7^{11} \quad e_8^{11} \quad e_9^{11} \quad e_{10}^{11} \quad e_{11}^{11} \quad e_{12}^{11}]^{\mathrm{T}}\end{aligned} \quad \text{and} \tag{7}$$

$$\begin{aligned}\mathbf{q}_n^{12} = [&e_1^{12} \quad e_2^{12} \quad e_3^{12} \quad e_4^{12} \quad e_5^{12} \quad e_6^{12} \\ &e_7^{12} \quad e_8^{12} \quad e_9^{12} \quad e_{10}^{12} \quad e_{11}^{12} \quad e_{12}^{12}]^{\mathrm{T}},\end{aligned} \tag{8}$$

where the transformation of Eq. (5) can be recognized as the first element in Eq. (9),

$$\mathbf{B}_1^{11} = \begin{bmatrix}
1&0&0&0&0&0&0&0&0&0&0&0&0&0&0&0&0&0\\
0&1&0&0&0&0&0&0&0&0&0&0&0&0&0&0&0&0\\
0&0&1&0&0&0&0&0&0&0&0&0&0&0&0&0&0&0\\
0&0&0&1&0&0&0&0&0&0&0&0&0&0&0&0&0&0\\
0&0&0&0&1&0&0&0&0&0&0&0&0&0&0&0&0&0\\
0&0&0&0&0&1&0&0&0&0&0&0&0&0&0&0&0&0\\
0&0&0&0&0&0&1&0&0&0&0&0&0&0&0&0&0&0\\
0&0&0&0&0&0&0&1&0&0&0&0&0&0&0&0&0&0\\
0&0&0&0&0&0&0&0&1&0&0&0&0&0&0&0&0&0\\
0&0&0&0&0&0&0&0&0&1&0&0&0&0&0&0&0&0\\
0&0&0&0&0&0&0&0&0&0&1&0&0&0&0&0&0&0\\
0&0&0&0&0&0&0&0&0&0&0&1&0&0&0&0&0&0
\end{bmatrix} \tag{9}$$

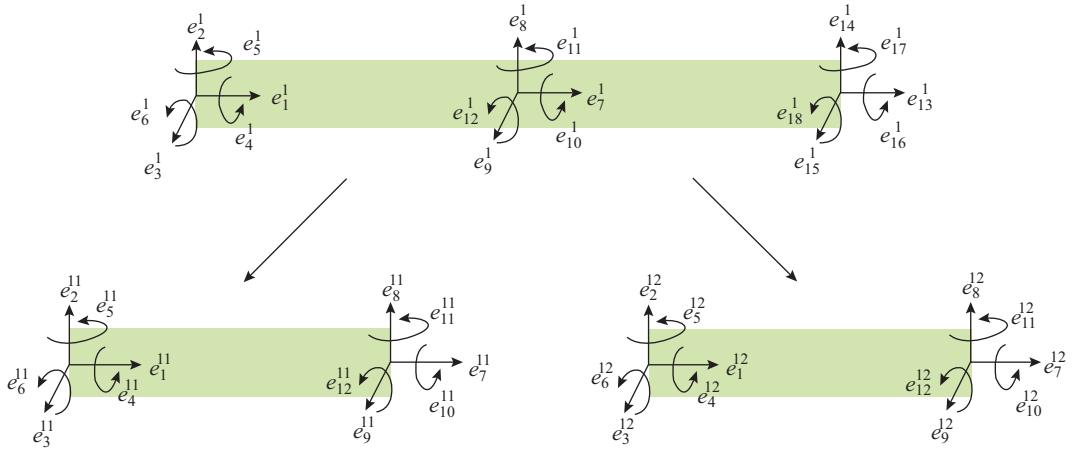

Fig. 4. Nodal coordinates defined in the body coordinates system.

and as the second element in Eq. (10).

$$\mathbf{B}_1^{12} = \begin{bmatrix} 0&0&0&0&0&0&1&0&0&0&0&0&0&0&0&0&0&0 \\ 0&0&0&0&0&0&0&1&0&0&0&0&0&0&0&0&0&0 \\ 0&0&0&0&0&0&0&0&1&0&0&0&0&0&0&0&0&0 \\ 0&0&0&0&0&0&0&0&0&1&0&0&0&0&0&0&0&0 \\ 0&0&0&0&0&0&0&0&0&0&1&0&0&0&0&0&0&0 \\ 0&0&0&0&0&0&0&0&0&0&0&1&0&0&0&0&0&0 \\ 0&0&0&0&0&0&0&0&0&0&0&0&1&0&0&0&0&0 \\ 0&0&0&0&0&0&0&0&0&0&0&0&0&1&0&0&0&0 \\ 0&0&0&0&0&0&0&0&0&0&0&0&0&0&1&0&0&0 \\ 0&0&0&0&0&0&0&0&0&0&0&0&0&0&0&1&0&0 \\ 0&0&0&0&0&0&0&0&0&0&0&0&0&0&0&0&1&0 \\ 0&0&0&0&0&0&0&0&0&0&0&0&0&0&0&0&0&1 \end{bmatrix} \tag{10}$$

Thus, the displacement of element *ij* in Eq. (4) in terms of the nodal coordinates of body *i* is as follows:

$$\bar{\mathbf{u}}^{ij} = \mathbf{C}^{ij}\mathbf{S}^{ij}\bar{\mathbf{C}}^{ij}\mathbf{B}_1^{ij}\mathbf{q}_n^i, \tag{11}$$

or in compact form, as follows:

$$\bar{\mathbf{u}}^{ij} = \mathbf{N}^{ij}\mathbf{q}_n^i, \tag{12}$$

wherein $\mathbf{N}^{ij}$ is defined as follows.

$$\mathbf{N}^{ij} = \mathbf{C}^{ij}\mathbf{S}^{ij}\bar{\mathbf{C}}^{ij}\mathbf{B}_1^{ij} \tag{13}$$

In the finite element formulation, the vector of the nodal coordinate of body i can be separated as follows:

$$\mathbf{q}_n^i = \mathbf{q}_o^i + \bar{\mathbf{q}}_f^i, \tag{14}$$

wherein $\mathbf{q}_o^i$ is the vector of the nodal coordinates in the undeformed state, and $\bar{\mathbf{q}}_f^i$ is the vector of the nodal deformation. Not all nodal coordinates have nodal deformation components due to the boundary condition. Thus, the vector of the nodal deformation can be written as follows:

$$\bar{\mathbf{q}}_f^i = \mathbf{B}_2^i\mathbf{q}_f^i, \tag{15}$$

wherein $\mathbf{q}_f^i$ is the new vector of the nodal deformation, a set of valid deformation components of $\bar{\mathbf{q}}_f^i$, and $\mathbf{B}_2^i$ is a linear transformation that matches elements of $\mathbf{q}_f^i$ to the nodal coordinate of the body.

Finally, the position vector of the arbitrary point of the deformable body with respect to the global coordinate system is as follows:

$$\begin{aligned} \mathbf{r}^{ij} &= \mathbf{R}^i + \mathbf{A}^i\bar{\mathbf{u}}^{ij} \\ &= \mathbf{R}^i + \mathbf{A}^i\mathbf{N}^{ij}\mathbf{q}_n^i \\ &= \mathbf{R}^i + \mathbf{A}^i\mathbf{N}^{ij}(\mathbf{q}_o^i + \mathbf{B}_2^i\mathbf{q}_f^i) \end{aligned}, \tag{16}$$

wherein $\mathbf{R}^i$ is the position vector of the orientation of the body coordinate system with respect to the global coordinate system, and $\mathbf{A}^i$ is the rotation matrix between the body coordinate system and the global coordinate system.

Differentiating Eq. (16) with respect to time yields the following equation:

$$\dot{\mathbf{r}}^{ij} = \dot{\mathbf{R}}^i - \mathbf{A}^i\tilde{\bar{\mathbf{u}}}^{ij}\bar{\mathbf{G}}^i\dot{\boldsymbol{\theta}}^i + \mathbf{A}^i\mathbf{N}^{ij}\mathbf{B}_2^i\dot{\mathbf{q}}_f^i, \tag{17}$$

wherein $\tilde{\bar{\mathbf{u}}}^{ij}$ is the skew matrix form of vector $\bar{\mathbf{u}}^{ij}$, and $\bar{\mathbf{G}}^i$ is the transformation matrix between the Euler angle and the angular velocity. Eq. (17) can be written in matrix form as follows:

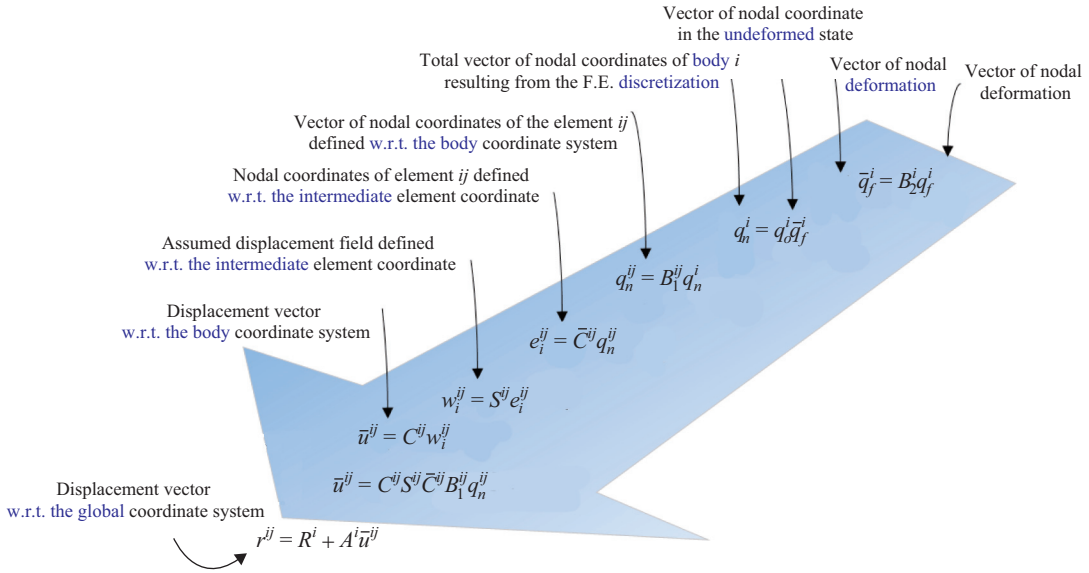

Fig. 5. Summary of the kinematic description of the flexible body.

$$\dot{\mathbf{r}}^{ij} = \begin{bmatrix} \mathbf{I} & -\mathbf{A}^i \tilde{\bar{\mathbf{u}}}^{ij} \bar{\mathbf{G}}^i & \mathbf{A}^i \mathbf{N}^{ij} \mathbf{B}_2^i \end{bmatrix} \begin{bmatrix} \dot{\mathbf{R}}^i \\ \dot{\boldsymbol{\theta}}^i \\ \dot{\mathbf{q}}_f^i \end{bmatrix} \tag{18}$$

Fig. 5 shows a summary of the kinematic description of the flexible body with their definition. This kinematic description method uses four different coordinate systems from the nodal coordinate system with respect to the body coordinate system to the global coordinate system via intermediate element coordinate system and element coordinate system.

2 Equations of Motion of a Flexible Multibody System

Using Eq. (18), the kinetic energy of a deformable body can be defined. The matrix $\mathbf{M}^{ij}$ defined in Eq. (19) is called "mass matrix," which is in turn defined in Eq. (20).

$$\begin{aligned} T^i &= \frac{1}{2} \int_{V^i} \rho^{ij} \dot{\mathbf{r}}^{ij\mathrm{T}} \dot{\mathbf{r}}^{ij} dV^{ij} \\ &= \frac{1}{2} \dot{\mathbf{q}}^{i\,\mathrm{T}} \mathbf{M}^{ij} \dot{\mathbf{q}}^i \end{aligned} \tag{19}$$

$$\mathbf{M}^{ij} = \int_{V^{ij}} \left(\rho^{ij} \begin{bmatrix} \mathbf{I} & -\mathbf{A}^i \tilde{\bar{\mathbf{u}}}^i \bar{\mathbf{G}}^i & \mathbf{A}^i \mathbf{N}^{ij} \mathbf{B}_2^i \\ & \bar{\mathbf{G}}^{i\,T} \tilde{\bar{\mathbf{u}}}^{i\,T} \tilde{\bar{\mathbf{u}}}^i \bar{\mathbf{G}}^i & \bar{\mathbf{G}}^{i\,T} \tilde{\bar{\mathbf{u}}}^i \mathbf{N}^{ij} \mathbf{B}_2^i \\ sym. & & \mathbf{B}_2^{i\,T} \mathbf{N}^{ij\,T} \mathbf{N}^{ij} \mathbf{B}_2^i \end{bmatrix} \right) dV^{ij} \tag{20}$$

Eq. (20) can be simplified as follows:

$$\mathbf{M}^{ij} = \begin{bmatrix} m_{RR} & m_{R\theta} & m_{Rf} \\ & m_{\theta\theta} & m_{\theta f} \\ sym. & & m_{ff} \end{bmatrix}^{ij}, \tag{21}$$

wherein m_{RR} is the inertia due to the mass of the body, $m_{\theta\theta}$ is the mass moment of the inertia due to rotational motion, and $m_{R\theta}$ is the inertia due to the coupling of translational and rotational motions. Terms m_{Rf}, $m_{\theta f}$, and m_{ff} are inertias due to deformation of the body.

Virtual work due to generalized elastic force can be defined as follows using deformation of the body $\mathbf{q}_f^i$:

$$\delta \mathrm{W}_s^i = -\mathbf{q}_f^{i\,\mathrm{T}} \mathbf{K}_{ff}^i \delta \mathbf{q}_f^i, \tag{22}$$

wherein $\mathbf{K}_{ff}^{ij}$ is the stiffness matrix. Shabana (2005) suggested the stiffness matrix of a two-dimensional (2D) beam element. Przemieniecki (1968) suggested the stiffness matrix of a 3D beam element.

To make a single equation of motion of a multibody system, all connections between bodies should be expressed as constraints. Such constraints are functions of the displacement $\mathbf{q}$ and the time t as shown in Eq. (23). Thus, the virtual work due to constraints force is defined as in Eq. (24):

$$\mathbf{C}(\mathbf{q}, t) = 0 \text{ and} \tag{23}$$

$$\mathbf{C}_\mathbf{q} \delta \mathbf{q} = 0, \tag{24}$$

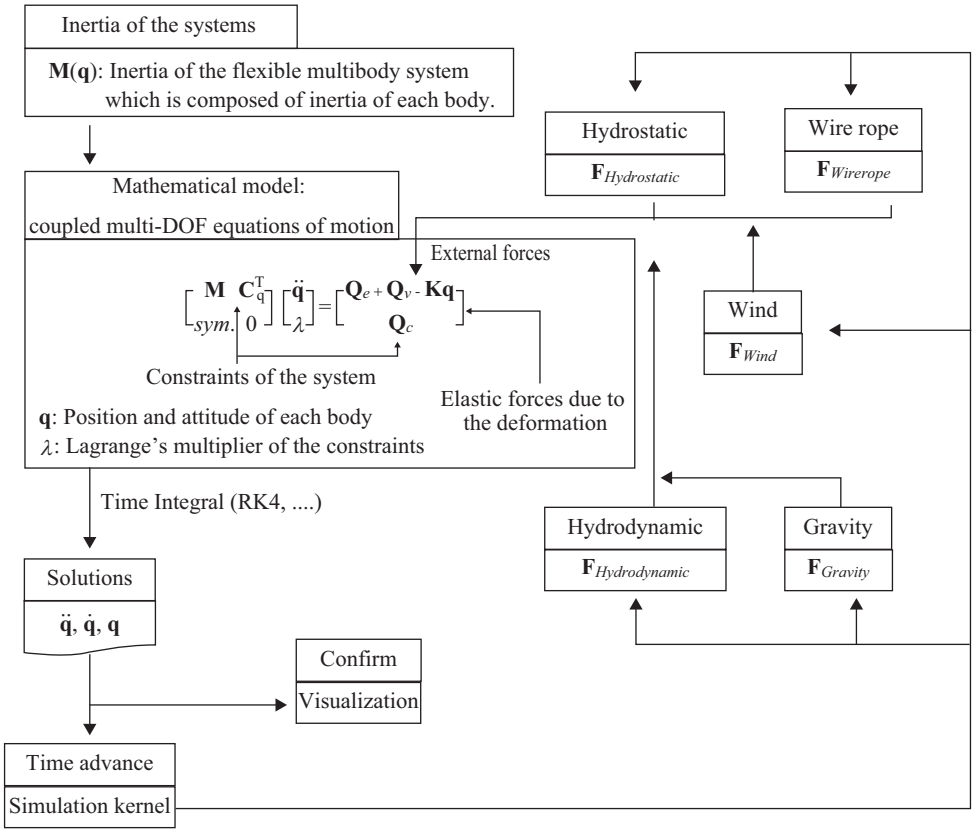

Fig. 6. General sequence of solutions of the equations of motion of the flexible multibody system.

wherein $\mathbf{C}_\mathbf{q}$ is a derivative of $\mathbf{C}(\mathbf{q},t)$ with respect to the vector of the system generalized coordinate $\mathbf{q}$.

Virtual force due to external forces is defined as in Eq. (25). Its matrix form is Eq. (26):

$$\delta \mathrm{W}_e^i = \mathbf{Q}_e^{i\,\mathrm{T}} \delta \mathbf{q}^i \text{ and} \tag{25}$$

$$\delta \mathrm{W}_e^i = \begin{bmatrix} (\mathbf{Q}_e^i)_R^{\mathrm{T}} & (\mathbf{Q}_e^i)_\theta^{\mathrm{T}} & (\mathbf{Q}_e^i)_f^{\mathrm{T}} \end{bmatrix} \begin{bmatrix} \delta \mathbf{R}^i \\ \delta \boldsymbol{\theta}^i \\ \delta \mathbf{q}_f^i \end{bmatrix}, \tag{26}$$

wherein $\mathbf{Q}_e^i$ is generalized external force.

The equations of motion of the flexible multibody system were derived from Lagrange's equation using Eqs. (19), (22), (24), and (25) as shown in Eq. (27):

$$\frac{d}{dt}\left(\frac{\partial T^i}{\partial \dot{\mathbf{q}}^i}\right)^T - \left(\frac{\partial T^i}{\partial \mathbf{q}^i}\right)^T + \mathbf{C}_\mathbf{q}\boldsymbol{\lambda} = -\mathbf{K}^i\mathbf{q}^i + \mathbf{Q}_e^i, \tag{27}$$

wherein $\boldsymbol{\lambda}$ is the vector of Lagrange's multiplier. The matrix form of Eq. (27) can be written as follows:

$$\begin{bmatrix} m_{RR}^i & m_{R\theta}^i & m_{Rf}^i \\ & m_{\theta\theta}^i & m_{\theta f}^i \\ sym. & & m_{ff}^i \end{bmatrix} \begin{bmatrix} \ddot{\mathbf{R}}^i \\ \ddot{\boldsymbol{\theta}}^i \\ \ddot{\mathbf{q}}_f^i \end{bmatrix} + \begin{bmatrix} 0 & 0 & 0 \\ 0 & 0 & 0 \\ 0 & 0 & \mathbf{K}_{ff} \end{bmatrix} \begin{bmatrix} \mathbf{R}^i \\ \boldsymbol{\theta}^i \\ \mathbf{q}_f^i \end{bmatrix} + \begin{bmatrix} \mathbf{C}_{\mathbf{R}^i}^{\mathrm{T}} \\ \mathbf{C}_{\boldsymbol{\theta}^i}^{\mathrm{T}} \\ \mathbf{C}_{\mathbf{q}_f^i}^{\mathrm{T}} \end{bmatrix} \lambda = \begin{bmatrix} (\mathbf{Q}_e^i)_R^{\mathrm{T}} \\ (\mathbf{Q}_e^i)_\theta^{\mathrm{T}} \\ (\mathbf{Q}_e^i)_f^{\mathrm{T}} \end{bmatrix} + \begin{bmatrix} (\mathbf{Q}_v^i)_R^{\mathrm{T}} \\ (\mathbf{Q}_v^i)_\theta^{\mathrm{T}} \\ (\mathbf{Q}_v^i)_f^{\mathrm{T}} \end{bmatrix}, \tag{28}$$

wherein $\mathbf{Q}_v^i$ is the quadratic velocity term derived from vectors in Eq. (27).

Reorganizing Equ. (28) into augmented formulation to solve equations of motion can yield the following form of the equation.

$$\begin{bmatrix} \mathbf{M} & \mathbf{C}_\mathbf{q}^{\mathrm{T}} \\ sym. & 0 \end{bmatrix} \begin{bmatrix} \ddot{\mathbf{q}} \\ \lambda \end{bmatrix} = \begin{bmatrix} \mathbf{Q}_e + \mathbf{Q}_v - \mathbf{K}\mathbf{q} \\ \mathbf{Q}_c \end{bmatrix} \tag{29}$$

Solving Eq. (29) through numerical integration using the fourth-order Runge-Kutta method can yield the position and velocity in each time step.

Fig. 6 shows the general sequence of solutions of the equations of motion of the flexible multibody system.

Table 2. Specifications of a 2D cantilever beam.

Item	Value
Length	10 m
Mass	795 kg
Young's modulus	210 GPa
Second moment of inertia	8.33 x 10^{-6} m^4
Density	7850 kg/m^3
Area	0.01 m^3
No. of elements	1~10

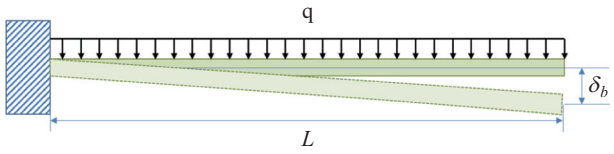

Fig. 7. Deformation of the 2D cantilever beam.

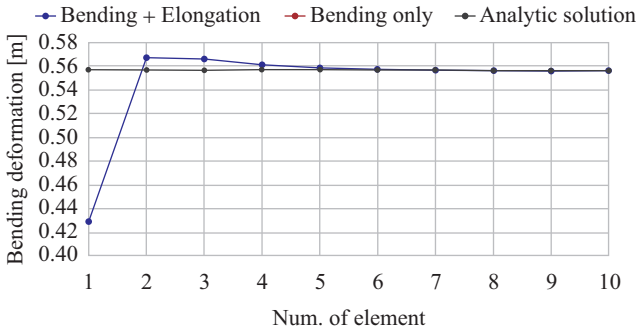

Fig. 8. Convergence test of the numerical cantilever beam model.

When the equations of motion are established as Eq. (29), the double time derivative of positions and the angle of system $\ddot{\mathbf{q}}$ are determined by solving the inverse matrix of Eq. (29). The position and angle of the system and its time derivative $\mathbf{q}$ and $\dot{\mathbf{q}}$ are obtained by integrating $\dot{\mathbf{q}}$ and $\ddot{\mathbf{q}}$ by an integrator such as the fourth-order Runge-Kutta method in each time step. The simulation kernel developed by Cha et al. (2010b) and Ha et al. (2015) can be used to calculate the elastic forces due to deformation and the external forces that act on the bodies such as hydrostatic forces, hydrodynamic forces, gravity, and wind forces in each time step to input the current value to solve the equations of motion.

III. COMPARATIVE STUDY OF FLEXIBLE MULTIBODY DYNAMICS FOR A 2D CANTILEVER BEAM

The analytic solution for the deformation of a 2D cantilever beam is used to validate the numerical model. The specifications of the 2D cantilever beam are listed in Table 2. The configuration of the model is shown in Fig. 7. Convergence test results of the numerical cantilever beam model are shown in Fig. 8.

The analytic solution of a 2D cantilever beam is as follows (Gere and Timoshenko, 1997):

$$\delta_b = \frac{qL^4}{8EI}, \tag{30}$$

wherein q is the uniform distributed load, L is the length of the beam, E is Young's modulus, and I is the second moment of inertia of the beam. The analytic solution is 0.0557 m. The result of the numerical analysis is converged to the analytic solution when the number of element is increased, suggesting that the numerical code has more reliable results than the analytic solution.

Table 3. Principal dimensions of Skandi Arctic.

Item	Value
LOA	156.9 m
LBP	137.7 m
Breadth	27 m
Depth of the first deck	12 m
Draft (design)	6.5 m
Draft (scantling)	8.5 m
Dead weight	10,996 tons @ 8.5 m

Table 4. Crane specifications of Skandi Arctic.

Item	Value
Type	Box boom crane
Main hoist capacity (harbor lift)	400 tons @ 11 m
Auxiliary hoist capacity	30 tons @ 46 m

IV. DYNAMIC SIMULATION OF THE LIFTING OPERATION OF AN OSV BASED ON FLEXIBLE MULTIBODY DYNAMICS

1. Simulation Model

Skandi Arctic is an OSV designed and built as a diving support and a heavy construction vessel. It provides saturation dive support as a heavy-lifting deck crane for offshore construction (Kupen, 2009). In this study, it was selected as the simulation target. The principal dimensions and the crane specifications (the main lifting facilities) of Skandi Arctic are shown in Tables 3 and 4, respectively. Its configuration and deck plan are shown in Fig. 9.

In this study, the subsea manifold lifting by Skandi Arctic was dynamically simulated in various ocean conditions to determine dynamic amplification factors of the lifted object using a simplified model of Skandi Arctic and the subsea manifold. The dynamic amplification factor is a ratio of the static load

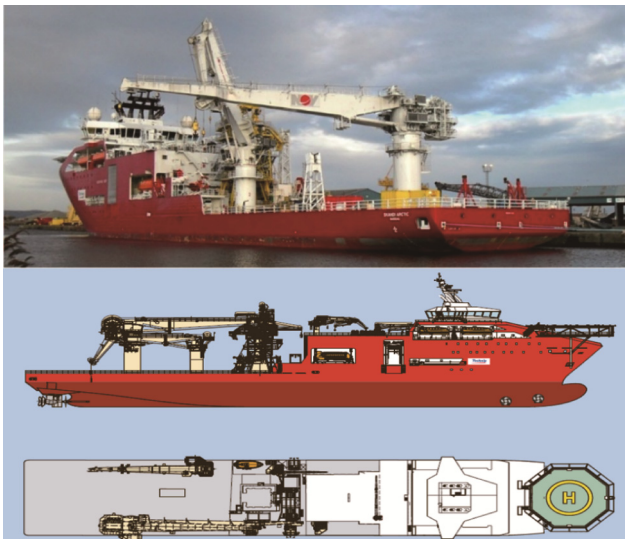

Fig. 9. The configuration and deck plan of Skandi Arctic (Kupen, 2009).

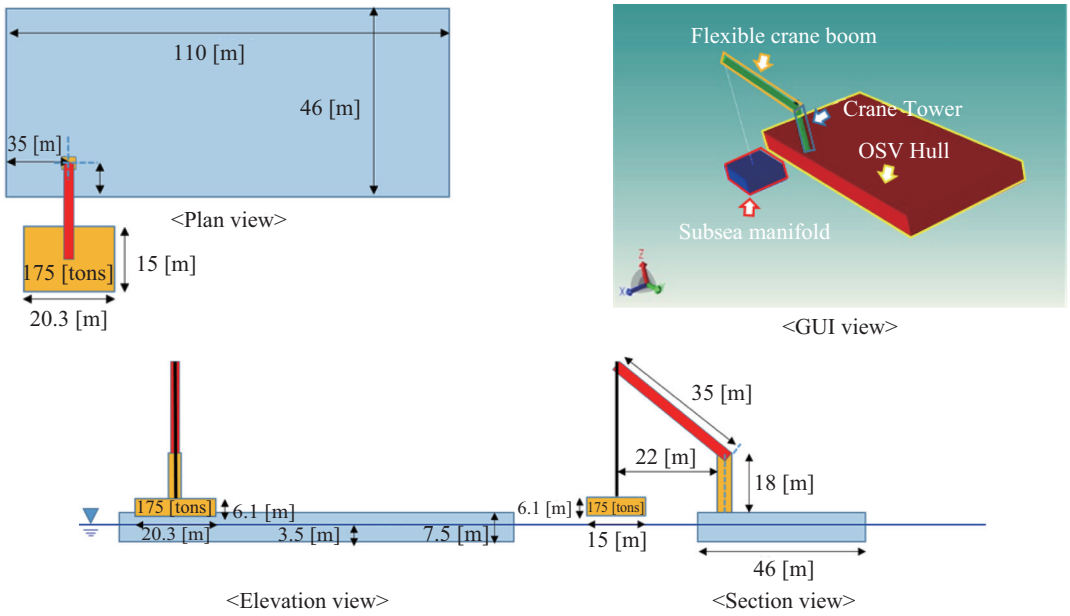

Fig. 10. Simplified simulation model of Skandi Arctic and the subsea manifold.

the dynamic load. The simplified model for the dynamic simulation is shown in Fig. 10. The specifications of the modeling data are shown in Table 5.

2. External Forces of the Simulated System

Gravity, hydrostatic forces, hydrodynamic forces, wind forces, and the reaction force of wire rope are the external forces of the simulated system. Gravity is the external force for all objects on earth. It basically acts at the center of the body. The center of gravity of a rigid body is a fixed point in the body coordinates system. However, the center of gravity of a flexible body can change due to deformation. Therefore, gravity that acts on the flexible body should be transformed to a generalized force as shown in Eqs. (25) and (26).

Wind forces on the load are considered as static forces as follows (Ku and Roh, 2015):

$$\mathbf{F}_{wind} = \frac{1}{2}\rho_{air} S V^2 , \tag{31}$$

wherein ρ_{air} is the density of air, S is the projected area of the load in the wind direction, and V is the wind velocity.

The hydrostatic forces on the hull are calculated as follows:

$$\mathbf{F}_{hydrostatic} = \rho_{SW}\, \mathbf{g} \nabla_{ship} , \tag{32}$$

Table 5. Specifications of the simplified modeling data.

Body	Item	Value
OSV hull	LOA	110 m
	Breadth	46 m
	Depth	7.5 m
	Draft	3.75 m
Crane	Type	Knuckle boom
	Capacity	400 tons @ 11 m
	Length of the boom	35 m
Subsea manifold (lifted object)	Length	20.3 m
	Breadth	15 m
	Depth	6.1 m
	Mass	175 tons

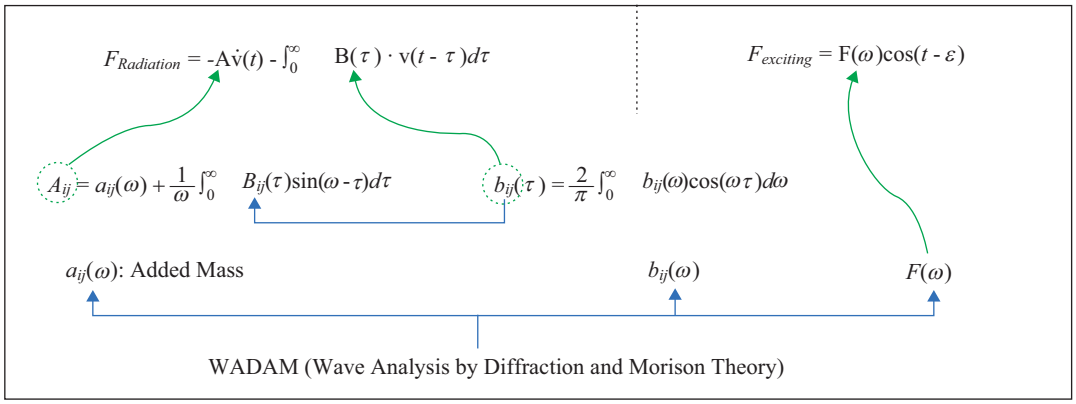

Fig. 11. Calculation procedure of hydrodynamic forces.

wherein ρ_{SW} is the density of sea water, g is the acceleration of gravity which is 9.81 m/s^2, and ∇_{ship} is the displacement volume of the ship. The kernel (Cha et al., 2010b) can be used to calculate the displacement volume in each time step to obtain the hydrostatic forces.

Hydrodynamic forces can be divided into wave-exciting force and radiation force as shown in Eq. (33). The waveexciting force is exerted by incident wave while the radiation force is generated by the motion of the floater itself.

$$\mathbf{F}_{hydrodynamic} = \mathbf{F}_{exciting} + \mathbf{F}_{radiation} \tag{33}$$

$\mathbf{F}_{exciting}$ is obtained from the force RAO (Response Amplitude Operator) and the sinusoidal function at a given frequency. The force RAO can be obtained from a commercial solver such as WADAM by DNV (Det Norske Veritas, 2002). To calculate $\mathbf{F}_{radiation}$ in the time domain, Cummins equation (Cummins, 1962) can be used. The added mass $a_{ij}(\omega)$ and the damping coefficient $b_{ij}(\omega)$ can also be obtained from the commercial solver. The calculation procedure is shown in Fig. 11.

For this simulation, hydrodynamic forces are pre-calculated with commercial hydrodynamics tool WADAM by DNV in the simulated draft (Det Norske Veritas, 2002). WADAM uses a 3D panel method to evaluate velocity potentials and hydrodynamic coefficients. The radiation and diffraction velocity potentials on the wet part of the body surface are determined from the solution of an integral equation that is obtained by using Green's theorem with free surface source potentials as Green's functions. The source strengths are evaluated based on source distribution method using the same source potentials. The velocity potential is the sum of incident wave potential, diffraction velocity potential, and radiation velocity potential. Hydrodynamic pressure on the hull is determined from Bernoulli's equation. The hydrodynamic force is obtained from the result of surface integral of the hydrodynamic pressure. Hydrodynamic force consists of Froude-Krylov force, diffraction force, and radiation force obtained from incident wave potential, diffraction velocity potential, and radiation velocity potential, respectively. From the calculated result of the radiation force, added mass coefficient and damping coefficient are obtained. Froude-Krylov force and diffraction force become wave exciting force. The reaction force of the wire rope is modeled as incompressible spring.

Table 6. Summary of simulation cases.

Case	Body type	Wave condition			
		Amplitude [m]	Period [sec]	Heading angle [deg]	Wind speed [m/s]
0	Flexible	0.0	0	0	0
1	Rigid	1.0	10.5	0	0
2					10
3				45	0
4				90	0
5	Flexible			0	0
6					10
7				45	0
8				90	0
9			14	0	0
10			12.5		
11			9		
12			8		
13			7		

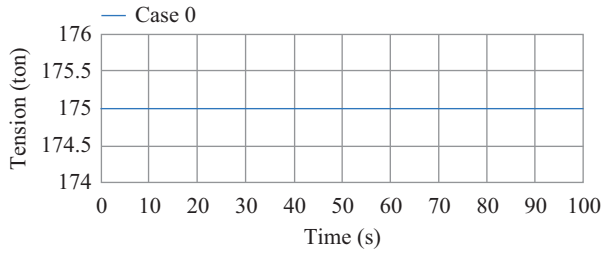

Fig. 12. Tension of the wire rope of case 0 (no hydrodynamic force at static equilibrium).

Thus, this wire rope equivalent spring can suggest the tension to the linked body. In the simulation, the wire rope force is measured as tension.

3. Simulation Results

Simulation was performed in 13 different cases with two different body types, six wave periods, three wave heading angles, and two wind speeds. The wave amplitude is fixed to one meter. These simulation cases are summarized in Table 6.

Case 0 is the case without hydrodynamic force at static equilibrium state. In this case, the tension of the wire-rope is the same as the weight of the lifted object as shown in Fig. 12. Therefore, dynamic amplification factor of case 0 is 1.0, which means that the dynamic amplification factor contributes to the hydrodynamic force.

Case 1 and 5, 3 and 7, and 4 and 8 are comparison between the rigid model and the flexible model at 0°, 45° and 90° wave heading angles, respectively. Dynamic amplification factor is a ratio of the maximum tension to static load. The maximum tension and dynamic amplification factor according to the body type and the wave heading angles are shown in Table 7. The dynamic amplification factor of the flexible boom model was bigger than that of the rigid model in all cases (Table 7). Tension of the wire rope according to body type and wave heading angle is shown in Fig. 13. Vertical position of the crane boom tip according to body type and wave heading angle is shown in Fig. 14.

Table 7. Maximum tension and dynamic amplification factor according to the body type and the wave heading angle.

Amplitude: 1.0 [m], Period: 10.5 [sec], Wind speed: 0 [m/s]					
Case	Body type	Heading angle [deg]	Maximum tension [ton]	Dynamic amplification factor	Maximum height of the motion oscillation [m]
1	Rigid	0	177.7	1.015	0.44
5	Flexible		209.9	1.199	1.57
3	Rigid	45	185.1	1.058	1.69
7	Flexible		216.0	1.234	2.72
4	Rigid	90	190.5	1.088	1.67
8	Flexible		214.3	1.225	1.86

The general behavior of flexible crane boom tip follows a rigid one with small perturbation due to its flexibility. However, peaks and valleys of the graph of the flexible crane tip is bigger than the rigid one caused by deformation of the crane boom due to the weight of the lifted object and its own weight. Comparison between case 1 and 5 shows big differences in both tension and motion. In this case, the maximum tension of case 1 is 177.7 ton while that of case 5 is 209.9 ton. The maximum height of motion oscillation of case 1 is 0.44 m while that of case 5 is 1.57 m. Comparison between case 3 and 7 or between case 4 and 8 shows the same result that the flexible model has higher maximum tension and oscillation height, indicating that the flexibility of the crane beam should be considered to ensure the safety and accuracy of crane lifting operation. However, comparison between wave heading angles of case 1, 3, 4 and those of case 5, 7, 8 shows different tendency. The rigid body has the maximum dynamic amplification factor at 90-degree heading angle. However, the flexible body has the maximum dynamic amplification factor at 45 degrees. There reason for the difference between rigid body and flexible body is currently unclear. This might be a non-linear behavior of the flexible body. Whether this might be true merits further studies.

The relative vertical position of the crane boom tip and the lifted object is shown in Fig. 15. The lifted object is linked to the wire rope to provide the same tension to the crane boom tip and the lifted object. Thus, the relative vertical position of the crane boom tip in case 1 is the same as the lifted object because the crane tip is rigid. However, in case 5, the relative vertical position of the lifted object generally follows the motion of the crane boom tip. Some perturbation can occur due

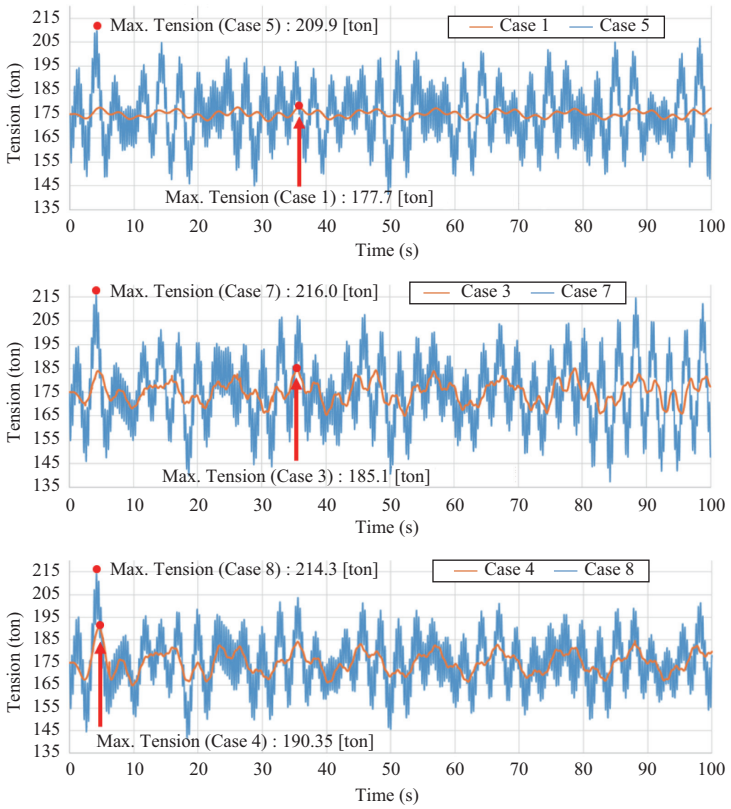

Fig. 13. Tension of the wire rope according to body type and wave heading angle.

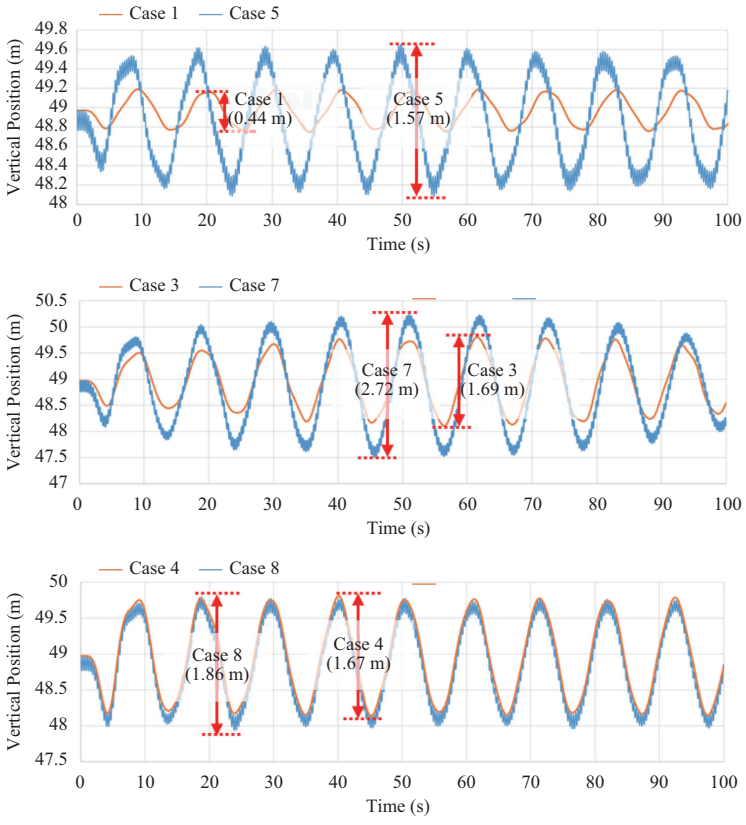

Fig. 14. Vertical position of the crane boom tip according to body type and wave heading angle.

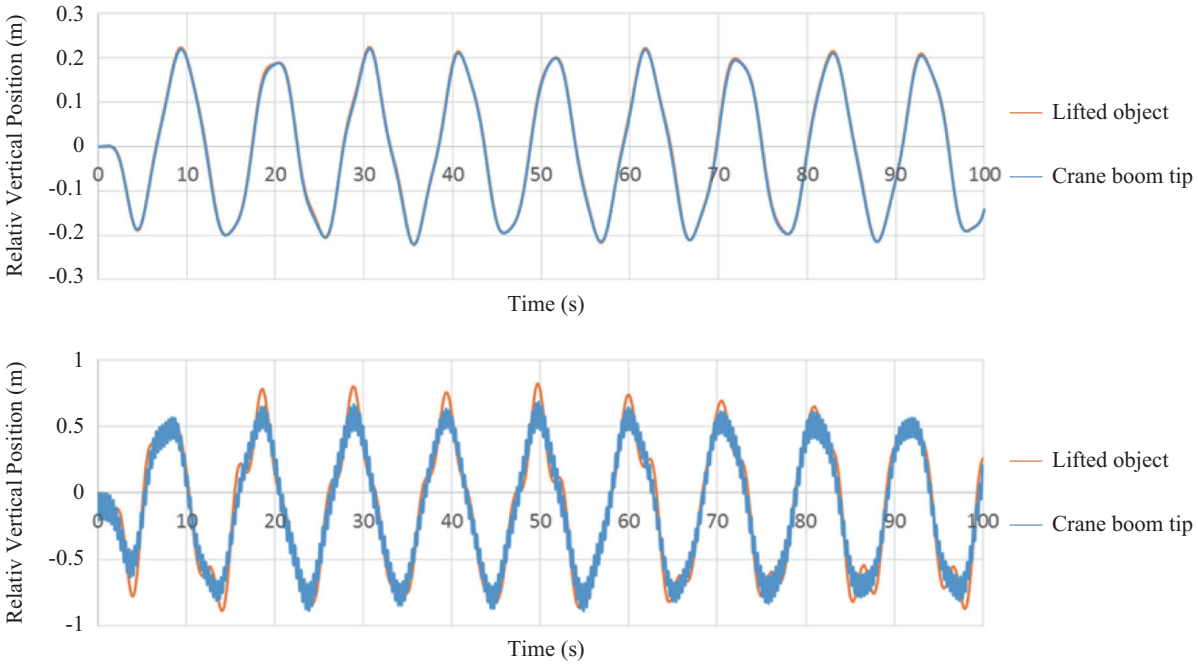

Fig. 15. Relative vertical position of the crane boom tip and the lifted object.

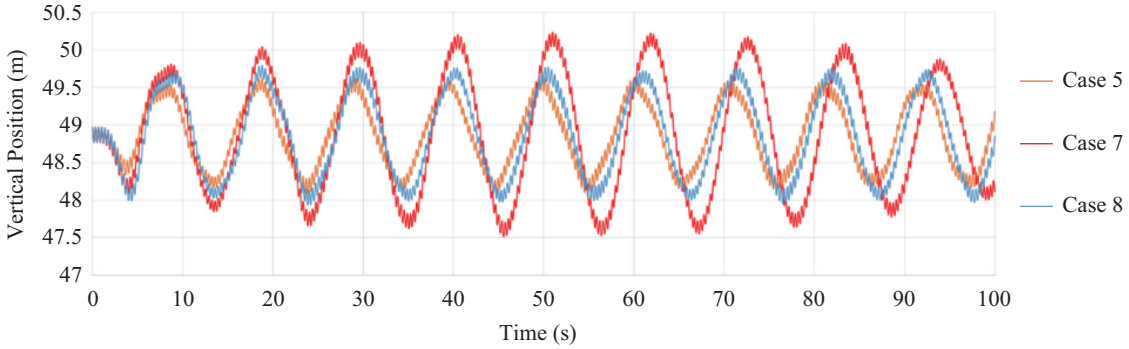

Fig. 16. Vertical position of the crane boom tip according to wave heading angle.

to vibration of the crane boom. Fig. 16 shows the behavior of the crane boom tip of flexible model according to wave heading angle. Case 7 shows the biggest behavior when the wave heading angle is 45 degrees.

Maximum tension and dynamic amplification factor according to wave period are shown in Table 8. The effect of wave period on dynamic behavior is observed in case 5, 9, 10, 11, 12, and 13. Tension of the wire rope according to wave period is shown in Fig. 17. Vertical position of the crane boom tip according to wave period is shown in Fig. 18.

The maximum tension load was maximized when the wave period was 12.5 seconds. The maximum height of motion oscillation was maximized when the wave period was 14 seconds, indicating that the resonance period of this system might be between 12.5 and 14 seconds. Maximum tension and dynamic amplification factor according to the wind force are summarized in Table 9.

Table 8. Maximum tension and dynamic amplification factor, according to wave period.

Amplitude: 1.0 [m], Heading angle: 0 [deg], Wind speed: 0 [m/s]					
Case	Body type	Wave period [sec]	Maximum tension [ton]	Dynamic Amplification factor	Maximum height of the motion oscillation [m]
5	Flexible	10.5	209.9	1.199	1.57
9		14	210.1	1.201	1.83
10		12.5	210.9	1.205	1.78
11		9	207.6	1.186	1.22
12		8	207.4	1.185	0.87
13		7	206.4	1.179	0.79

Wind forces slightly increased the maximum tension and

Table 9. Maximum tension and dynamic amplification factor, according to wind speed.

Amplitude: 1.0 [m], Period: 10.5 [sec], Heading angle: 0 [deg]					
Case	Body type	Wind speed [m/s]	Maximum tension [ton]	Dynamic Amplification factor	Maximum height of the motion oscillation [m]
1	Rigid	0	177.7	1.015	0.44
2		10	177.8	1.016	0.44
5	Flexible	0	209.8	1.199	1.57
6		10	209.9	1.199	1.58

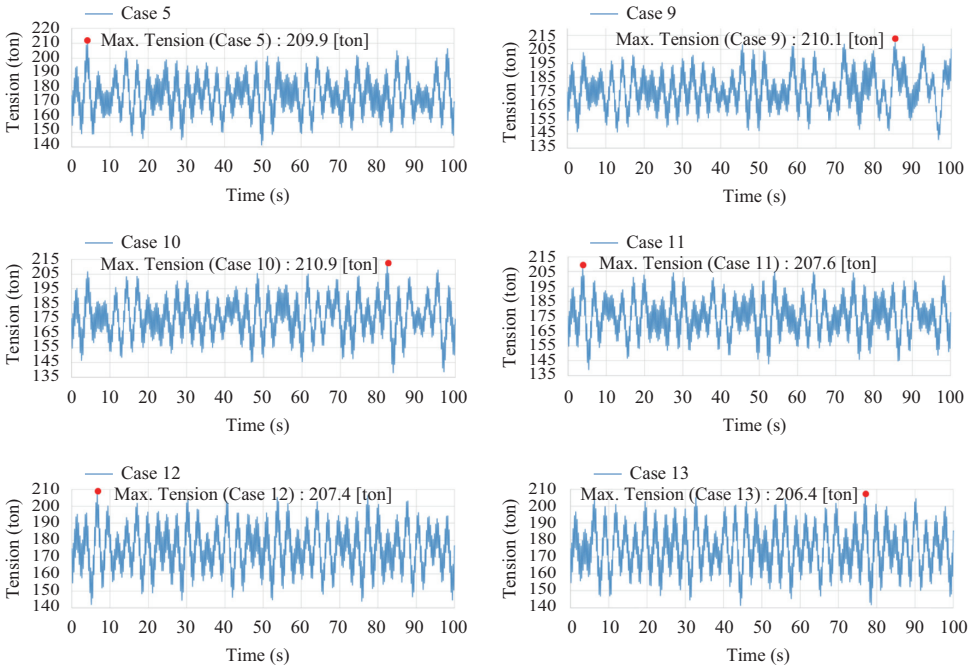

Fig. 17. Tension of the wire rope according to wave period.

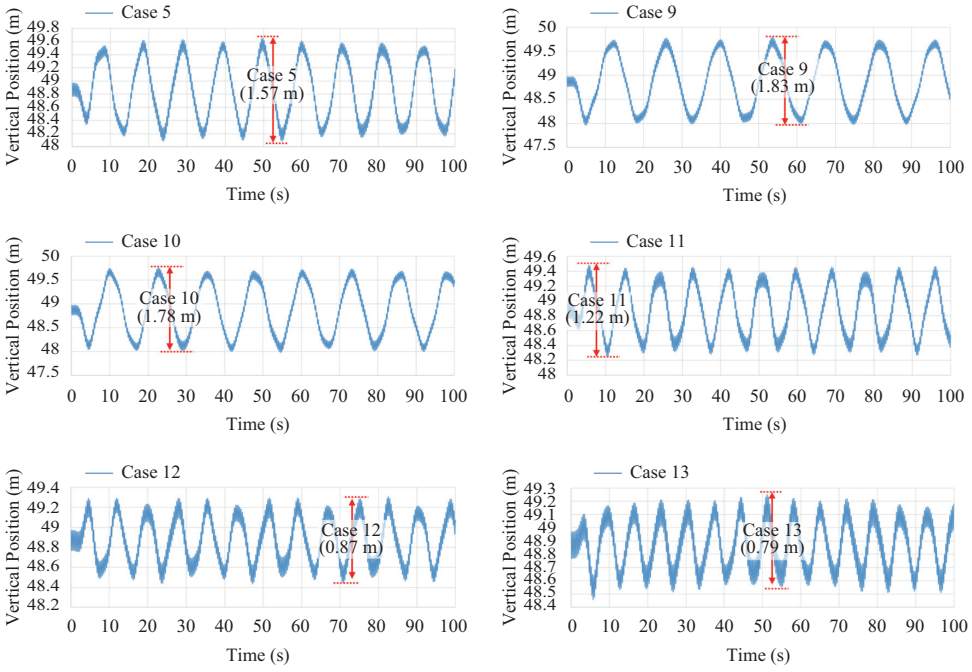

Fig. 18. Vertical position of the crane boom tip according to wave period.

the dynamic amplification factor. If the wind speed and the project area of the lifting object are increased, the maximum tension and the dynamic amplification factor are also increased. Based on simulation results, the flexible analysis yielded more accurate dynamic amplification factors that could hedllp produce a reasonable safety margin and guidelines for crane operation.

V. CONCLUSIONS AND FUTURE STUDIES

The crane-lifting function of an OSV was simulated in this study using flexible multibody dynamics. The crane-lifting performance of the OSV under various ocean environments was modeled as a flexible multibody system consisting of a rigid OSV hull structure with hydrodynamic and hydrostatic forces, a rigid crane tower attached to the hull, a finite-element-modeled flexible crane boom attached to the crane tower, a rigid modeled load, and a wire rope modeled with a spring. The hydrodynamic forces were pre-calculated using WADAM tool and the wind forces were considered for the load.

The result of the simulation showed that flexible models had a bigger dynamic amplification factor than rigid models in all cases, suggesting that the flexibility of the crane boom should be considered to accurately estimate dynamic effect on crane-lifting. In addition, the simulation result revealed severe conditions for crane operation so that guidelines for crane operation in certain ocean conditions can be generated.

For future studies, proper verification for lifting operation of an OSV will be performed. However, there is no reliable commercial code that can reproduce the same example of this study. Therefore, a simplified example that can replace the hydrodynamic effect on the ship is needed in future studies by making forced oscillation on the ship. Otherwise, model test can be performed for verification purpose.

For the next step, the scenario function that can simulate subsequent events will be added to simulate deck lifting to lowering through splash zone. To do this, a study on splash zone effect is required. Next, improved wire rope model will be applied based on the constraints of wire rope model that show the realistic behavior of the wire rope. The final goal is to apply finite element structural analysis to dynamic analysis to not only see the dynamic response, but also check the structural response of the body component.

ACKNOWLEDGMENTS

This study was partially supported by (a) BK21 Plus Program (Education and Research Center for Creative Offshore Plant Engineers) funded by the Ministry of Education of the Republic of Korea; and (b) Research Institute for Marine Systems Engineering of Seoul National University, Republic of Korea.

APPENDIX

A1. Explicit Expressions for Matrices

Element shape function $\mathbf{S}^{ij}$ is defined as:

$$\mathbf{S}^{ij\mathrm{T}} = \begin{bmatrix} 1-\xi & 0 & 0 \\ 6\left(\xi-\xi^2\right)\eta & 1-3\xi^2+2\xi^3 & 0 \\ 6\left(\xi-\xi^2\right)\zeta & 0 & 1-3\xi^2+2\xi^3 \\ 0 & -\left(1-\xi\right)l\zeta & -\left(1-\xi\right)l\eta \\ \left(1-4\xi+3\xi^2\right)l\zeta & 0 & \left(-\xi+2\xi^2-\xi^3\right)l \\ \left(-1+4\xi-3\xi^2\right)l\eta & \left(\xi-2\xi^2+\xi^3\right)l & 0 \\ \xi & 0 & 0 \\ 6\left(-\xi+\xi^2\right)\eta & 3\xi^2-2\xi^3 & 0 \\ 6\left(-\xi+\xi^2\right)\zeta & 0 & 3\xi^2-2\xi^3 \\ 0 & -l\xi\zeta & -l\xi\eta \\ \left(-2\xi+3\xi^2\right)l\zeta & 0 & \left(\xi^2-\xi^3\right)l \\ \left(2\xi-3\xi^2\right)l\eta & \left(-\xi^2+\xi^3\right)l & 0 \end{bmatrix},$$

where

$$\xi = \frac{x_1^{ij}}{l^{ij}},\ \eta = \frac{x_2^{ij}}{l^{ij}},\ \zeta = \frac{x_3^{ij}}{l^{ij}}$$

l^{ij} is the length of element ij, x_1^{ij}, x_2^{ij}, and x_3^{ij} are spatial coordinates along element axes.

Rotation matrix $\mathbf{C}^{ij}$ is defined as:

$$\mathbf{C}^{ij} = \begin{bmatrix} c_1 & \dfrac{-c_1c_2}{\sqrt{\left(c_1\right)^2+\left(c_3\right)^2}} & \dfrac{-c_3}{\sqrt{\left(c_1\right)^2+\left(c_3\right)^2}} \\ c_2 & \sqrt{\left(c_1\right)^2+\left(c_3\right)^2} & 0 \\ c_3 & \dfrac{-c_2c_3}{\sqrt{\left(c_1\right)^2+\left(c_3\right)^2}} & \dfrac{c_1}{\sqrt{\left(c_1\right)^2+\left(c_3\right)^2}} \end{bmatrix}$$

where

$$c_1^{ij} = \frac{b_1-a_1}{l^{ij}},\ c_2^{ij} = \frac{b_2-a_2}{l^{ij}},\ c_3^{ij} = \frac{b_3-a_3}{l^{ij}}$$

The locations of the nodes of element ij are defined as $\left(a_1, a_2, a_3\right)$ and $\left(b_1, b_2, b_3\right)$.

Transformation matrix $\overline{\mathbf{C}}^{ij}$ is defined as:

$$\overline{\mathbf{C}}^{ij} = \begin{bmatrix} \mathbf{C}^{ij} & 0 & 0 & 0 \\ 0 & \mathbf{C}^{ij} & 0 & 0 \\ 0 & 0 & \mathbf{C}^{ij} & 0 \\ 0 & 0 & 0 & \mathbf{C}^{ij} \end{bmatrix}^{\mathrm{T}}$$

Stiffness matrix of the beam element $\bar{\mathbf{K}}^{ij}$ is defined as:

$$\bar{\mathbf{K}}^{ij} = \begin{bmatrix}
\frac{Ea}{l} & & & & & & & & & & & \\
0 & \frac{12EI_3}{l^3} & & & & & & & & & & \\
0 & 0 & \frac{12EI_2}{l^3} & & & & & & & & & \\
0 & 0 & 0 & \frac{GJ}{l} & & & & & & & & \\
0 & 0 & \frac{6EI_2}{l^2} & 0 & \frac{4EI_2}{l} & & & & & & & \\
0 & \frac{6EI_3}{l^2} & 0 & 0 & 0 & \frac{4EI_3}{l} & & & & & & \\
-\frac{Ea}{l} & 0 & 0 & 0 & 0 & 0 & \frac{aE}{l} & & & & & \\
0 & -\frac{12EI_3}{l^3} & 0 & 0 & 0 & -\frac{6EI_3}{l^2} & 0 & \frac{12EI_3}{l^3} & & & & \\
0 & 0 & -\frac{12EI_2}{l^3} & 0 & \frac{6EI_2}{l^2} & 0 & 0 & 0 & \frac{12EI_2}{l^3} & & & \\
0 & 0 & 0 & -\frac{GJ}{l} & 0 & 0 & 0 & 0 & 0 & \frac{GJ}{l} & & \\
0 & 0 & -\frac{6EI_2}{l^2} & 0 & \frac{2EI_2}{l} & 0 & 0 & 0 & \frac{6EI_2}{l^2} & 0 & \frac{4EI_2}{l} & \\
0 & \frac{6EI_3}{l^2} & 0 & 0 & 0 & \frac{2EI_3}{l} & 0 & -\frac{6EI_3}{l^2} & 0 & 0 & 0 & \frac{4EI_3}{l}
\end{bmatrix}$$

Sym.

where, E^{ij} and G^{ij} are the modulus of elasticity and the modulus of rigidity of element *ij* respectively, J is the polar moment of the area, and I_2^{ij}, and I_3^{ij} are the second moment of area about the $\mathbf{X}_2^{ij}$, $\mathbf{X}_3^{ij}$ element axes, respectively. Further details are described in Shabana (2005).

REFERENCES

Al-Sweiti, Y. and D. Soffker (2007). Cargo pendulation suppression of ship cranes with elastic booms. Mathematical and Computer Modelling of Dynamical Systems 13, 503-529.

Cha, J. H., M. I. Roh and K. Y. Lee (2010a). Dynamic response simulation of a heavy cargo suspended by a floating crane based on multibody system dynamics. Ocean Engineering 37, 1273-1291.

Cha, J. H., M. I. Roh and K. Y. Lee (2010b). Integrated simulation framework for the process planning of ships and offshore structures. Robotics and Computer-Integrated Manufacturing Journal 26(5), 430-453.

Cummins, W. E. (1962). The impulse response function and ship motions. Schiffstechnik 9, 101-109.

Det Norske Veritas (2002). WADAM (Wave Analysis by Diffraction and Morison) theory. SESAM's user manual.

Gere, J. M. and S. P. Timoshenko (1997). Mechanics of materials, 4th edition, PWS Publishing.

Ha, S., N. K. Ku, M. I. Roh and H. J. Hwang (2015). Multibody system dynamics simulator for process simulation of ships and offshore plants in shipyards. Advances in Engineering Software 85, 12-25.

Ku, N. K. and M. I. Roh (2015). Dynamic response simulation of an offshore wind turbine suspended from a floating crane. Ships and Offshore Structures 10(6), 621-634.

Kupen, V. (2009). The different phases of a subsea lift from an offshore construction vessel. Proceedings of Subsea Lifting Operations Conference, Stavanger, Norway, 1-48.

Halse, K. H., V. Æsøy, D. Ponkratov, Y. Chu, J. Xu and E. Pedersen (2014). Lifting operations for subsea installations using small construction vessels and active heave compensation systems: A simulation approach. Proceedings of the 33rd International Conference on Ocean, Offshore, and Arctic Engineering, San Francisco, California, USA, 1-11.

Park, K. P., J. H. Cha and K. Y. Lee (2010). Lifting analysis considering the three-dimensional dynamics responses of a boom based on finite element formulation. Transactions of the Korean Society for Noise and Vibration Engineering 20, 753-760.

Park, K. S., M. S. Kim, Y. H. Ahn, M. J. Park, J. A. Lee and W. J. Kim (2012). Measures to encourage OSV (Offshore Support Vessel) market entrance for national wealth creation. Korea Maritime Institute, Republic of Korea.

Przemieniecki, J. S. (1968). Theory of matrix structural analysis. New York, McGraw-Hill Book Company.

Ren, H., X. Wang, Y. Hu and C. Li (2008). Dynamic response analysis of a moored crane ship with a flexible boom. Journal of Zhejiang University SCIENCE A 9, 29-31.

Shabana, A. A. (2005). Dynamics of multibody systems, 3rd edition. New York: Cambridge University Press.

Woo, J. H., J. H. Nam and K. H. Ko (2014). Development of a simulation method for the subsea production system. Journal of Computational Design and Engineering 1(3), 173-186.